BMC Medical Imaging

RESEARCH Open Access

Comparison of diagnostic performance for pulmonary nodule detection between free-breathing spiral ultrashort echo time and free-breathing radial volumetric interpolated breath-hold examination

Yehai Jiang[1,3], Doudou Pu[2], Xuyang Zhang[2], Zhanli Ren[2] and Nan Yu[1,2*]

Abstract

Objective This study aims to evaluate the efficacy of two free-breathing magnetic resonance imaging (MRI) sequences—spiral ultrashort echo time (spiral UTE) and radial volumetric interpolated breath-hold examination (radial VIBE).

Methods Patients were prospectively enrolled between February 2021 and September 2022. All participants underwent both 3T MRI scanning, utilizing the radial VIBE sequence and spiral UTE sequence, as well as standard chest CT imaging. The CT and MRI examinations were conducted within a 7-day interval. Two radiologists assessed the image quality using a visual 5-point ordinal Likert scale, and pulmonary nodules identified on MRI were evaluated through comparison with CT as the reference standard.

Results A total of 52 patients participated in this study, during which 82 pulmonary nodules were detected via CT imaging. The image quality scores for depicting pulmonary vasculature and airways using the spiral UTE sequence (4.61 ± 0.63; 4.76 ± 0.48) were significantly higher than those for the radial VIBE sequence (4.27 ± 0.87; 4.14 ± 0.82) ($P < 0.05$). However, for nodules smaller than 6 mm, the detection rate for the spiral UTE sequence (82.61%) was notably higher than that of the radial VIBE sequence (39.13%) ($P < 0.05$). Additionally, the detection rate for ground-glass nodules was higher with the spiral UTE sequence (75.00%) compared to the radial VIBE sequence (17.86%) ($P < 0.05$). The Pearson correlation coefficient (r) between radial VIBE and CT was 0.99 ($P < 0.001$), and the Pearson correlation coefficient (r) between spiral UTE and CT was also 0.99 ($P < 0.001$).

Conclusion The spiral UTE sequence demonstrates superior capability in visualizing ground glass nodules, blood vessels, and airways. In cases where patients present with ground glass nodules, the spiral UTE sequence is the preferred choice. Conversely, when the nodules are solid or partially solid, it is advisable to opt for radial VIBE sequences that are time-efficient and exhibit fewer artifacts.

*Correspondence:
Nan Yu
yunan0512@sina.com

Full list of author information is available at the end of the article

Keywords Ultrashort echo time, Free-breathing, Magnetic resonance imaging, Lung nodules

Background

In 2020, the Fleischner Society proposed the application of expanded lung magnetic resonance imaging (MRI) in the clinical practice. In recent years, MRI has increasingly been utilized for the evaluation of various conditions, including lung cancer staging [1, 2], lung nodules [3, 4], pulmonary hypertension [5], cystic fibrosis [6], chronic obstructive pulmonary disease [7], and interstitial lung disease [8]. Numerous imaging sequences have been reported for lung MRI, such as T2-weighted imaging(T2WI) half-fourier acquisition single-shot turbo spin-echo (HASTE) [9], T1-weighted imaging(T1WI) three-dimensional gradient echo (GRE) [10, 11] and ultrashort echo time (UTE) imaging [12]. Yu [13]found that free-breathing radial volumetric interpolated breath-hold examination (radial VIBE) was effective for assessing nodule morphology, with a detection rate of 95.7% for nodules using the radial VIBE sequence. In addition, the free-breathing UTE sequence has demonstrated a sensitivity of 90.8% for nodule detection, an accuracy of 87.7%, and a positive predictive value of 96.2% [14]. The UTE sequence has also been described as a valuable T1WI option for chest MRI in patients with poor breath-holding capability [12].

The range of lung MRI scanning is extensive; however, some patients exhibit poor lung function, limiting their ability to hold their breath for prolonged periods. In this context, free-breathing radial VIBE and UTE sequences can capture images during normal respiration. Prior literature has indicated that both radial VIBE and spiral UTE free-breathing sequences demonstrate favorable nodule detection rates. Nevertheless, there is a lack of studies addressing the differences between these two free-breathing sequences concerning pulmonary nodule detection. Additionally, there are few studies that evaluate the image quality of these sequences, complicating the selection for clinical applications. Therefore, this study aims to compare the image quality, nodule detection capabilities, and nodule size measurement accuracy of the radial VIBE sequence and the spiral UTE sequence, thereby offering valuable insights and guidance for clinical practice.

Materials and methods

Study design and patients

Between February 2021 and September 2022, patients with lung nodules detected on CT imaging and scheduled for pleural puncture were prospectively enrolled. The inclusion criteria consisted of: (1) patients with nodules detected on CT images; and (2) patients who required puncture or surgical biopsy. The exclusion criteria included: (1) Those suffering from respiratory problems such as dyspnea and contraindications to MRI, such as pacemakers, metal implants, and severe claustrophobia; (2) patients whose CT and MRI images were of inadequate quality to fulfill diagnostic requirements. The patients underwent chest CT and MRI within 7 days. The chest MRI utilized radial VIBE and spiral UTE sequences, both of which are free-breathing sequences. CT imaging served as the reference standard. This study received ethical approval from the affiliated hospital of Shaanxi University of Chinese Medicine, and all participants provided informed consent for MRI scans.

MRI acquisition

MRI was conducted using a 3 Tesla MR scanner (MAGNETOM Skyra, Siemens Healthcare, Erlangen, Germany) equipped with an 18-element body surface coil. All patients were positioned head-first and supine during the scanning process. The MRI scanning range extended from the thoracic inlet to 2 cm below the diaphragm. The chest MRI comprised radial VIBE and spiral UTE sequences, both of which are free-breathing sequences. Selected parameters for the applied sequences are presented in Table 1.

CT acquisition

CT scans were performed using a 64-multidetector row scanner (Discovery CT 750 HD, GE Healthcare, USA) during an end-inspiratory breath-hold, without the use of a contrast medium. The scanning range extended from the thoracic inlet to 2 cm below the diaphragm. The scanning parameters included an instantaneous tube voltage switch of 80/140 kV, a tube current of 260 mA, a rotation time of 0.5 s per rotation, and a matrix size of 512 × 512. The images were reconstructed in both axial and coronal orientations with a slice thickness of 1.25 mm.

Image analysis

The nodules were evaluated independently by two radiologists with 5 and 7 years of experience in thoracic radiology. To minimize detection bias, the observation procedure was as follows: (1) The results of the image quality evaluation of the MRI were compared with the CT images on a one-to-one basis. Both CT and MRI images were displayed simultaneously on a diagnostic

Table 1 Parameters of the applied MRI sequences

Parameters	Radial VIBE	Spiral UTE
TR (ms)	2.79	4.37
TE (ms)	1.39	0.05
Flip angle (°)	5°	4°
Fov (mm)	380	380
matrix	320 × 320	320 × 320
Acquired orientation	transversal	transversal
Slice thickness (mm)	1.2	3
Respiratory state	free breathing	free breathing
Acquisition time (s)	330s	480–540 s, depending on the patient's breathing pattern

MR, magnetic resonance imaging; VIBE, volumetric interpolated breath-hold examination; UTE, ultrashort echo time; TR, repetition time; TE, echo time

Table 2 Image quality scoring criteria

score	1	2	3	4	5
contrast	unacceptable	poor	acceptable	good	excellent
sharpness	unreadable	extreme blur	moderate blur	mild blur	no blur
pulmonary vascular	unacceptable	poor	acceptable	good	excellent
pulmonary airways	unacceptable	poor	acceptable	good	excellent
artifacts	unreadable	extreme artifacts	moderate artifacts	mild artifacts	no artifacts
Overall image quality	unacceptable	poor	acceptable	good	excellent

workstation. The assessment was based on six criteria: overall image quality, contrast, sharpness, pulmonary vascular, pulmonary airways and the presence of motion artifacts. Image quality was scored using a 5-point ordinal Likert scale, as detailed in Table 2 [15]. (2) The radiologists were instructed to record all visible pulmonary nodules on the MRI images. Any discrepancies between the two radiologists were resolved through consensus. (3) The two radiologists subsequently reviewed and recorded all visible pulmonary nodules on the CT images two weeks after the MRI reading, with any discrepancies again resolved by consensus. To evaluate nodule detection by MRI within each subgroup, nodules were classified into solid nodules, part-solid nodules, and ground-glass nodules. The detection rate for each MRI sequence was defined as the ratio of nodules detected by MRI to the total number of nodules identified in the CT scans. The size of the nodules on both CT and MRI images was measured based on the maximum diameter of the nodules' plane, with the final diameter calculated as the average of the measurements from the two radiologists. The results from the CT scans served as the reference standard.

Statistical analysis

Statistical analyses were performed using the SPSS 26.0 (SPSS, version 26.0, Chicago, IL, USA). The Wilcoxon test was used to evaluate the image quality scores of the sequences. The McNemar test was used to compare the two sequences for nodule detection. The differences between nodule sizes measured on CT and MRI images were evaluated using Pearson's linear regression correlation analysis. Inter-sequence and inter-reader agreements were determined using Cohen's kappa test. Bland–Altman plots were generated to depict inter-reader and inter-modality variances and limits of agreement visually. A P value < 0.05 was considered to be statistically significant.

Results

Patient and nodule characteristics

A total of 52 patients were enrolled in this study, resulting in the detection of 82 pulmonary nodules via CT. Among these nodules, 23 (28.05%) had a diameter of less than 6 mm, 22 (26.83%) ranged from 6 to 10 mm, and 37 (45.12%) exceeded 10 mm in diameter. The results of nodule detection using CT are presented in Table 3.

Image evaluation of MRI sequences for pulmonary nodules

As demonstrated in Table 4, spiral UTE images received higher subjective image quality scores for depicting pulmonary vasculature and airways (4.61 ± 0.63; 4.76 ± 0.48) compared to the radial VIBE sequence (4.27 ± 0.87; 4.14 ± 0.82) ($P < 0.05$). Conversely, radial VIBE images were rated higher for image artifact (4.03 ± 0.42) when compared to the spiral UTE sequence (3.71 ± 0.65) ($P < 0.05$). No significant differences were observed in image contrast, sharpness, or overall image quality between the two sequences (all $P > 0.05$). Representative images for evaluation are presented in Fig. 1.

Table 3 Patient and nodule characteristics

Patient (*n* = 52)	
Median age (range) in years	61.50(41–82)
Gender (Male/Female)	43/9
Nodule	82
Number of nodules per size category	
diameter≤6 mm	23
6 < diameter < 10 mm	22
diameter ≥ 10 mm	37
Number of nodules per location	
RUL	21
RML	13
RLL	19
LUL	21
LLL	8
Number of nodules per morphology category	
Solid	44
Part-solid	10
Non-solid	28

RUL, right upper lung; RML, right middle lung; RLL, right lower lung; LUL, left upper lung; LLL, left lower lung

Detection of pulmonary nodules

A total of 72 nodules were identified using spiral UTE, while 54 nodules were detected with the radial VIBE sequence. For nodules measuring less than 6 mm, the detection rate of the spiral UTE sequence (82.61%) was significantly higher than that of the radial VIBE sequence (39.13%) ($P<0.05$). Additionally, the detection rate for non-solid nodules was significantly higher when using the spiral UTE sequence (75.00%) compared to the radial VIBE sequence (17.86%) ($P<0.05$). The detection rates for solid nodules were 93.18% for the radial VIBE sequence and 94.45% for the spiral UTE sequence, demonstrating no significant difference ($P>0.05$). Furthermore, there were no notable differences in the detection rates of nodules located in various positions between the two sequences (all $P>0.05$). The characteristics and detection rates of pulmonary nodules are detailed in Table 5, and representative images of these nodules are presented in Fig. 2.

Among the nodules not detected by spiral UTE, ground glass nodules comprised 74%, with the majority located in the upper or middle lung regions. The nodules not identified in the radial VIBE sequence, 88% were ground glass nodules.

Nodule size between CT and MRI measurements

The nodule sizes measured on spiral UTE (mean, 11.64 ± 6.54 mm) and radial VIBE (mean, 11.36 ± 6.59 mm) were slightly smaller than those measured on CT (mean, 11.98 ± 6.40 mm) ($P>0.05$). The Pearson correlation coefficient (r) between radial VIBE

Table 4 Image evaluation of MRI sequences for pulmonary nodules

Scores (mean ± SD)	**CT**	**Radial VIBE**	**Spiral UTE**	***Z***	***P* Value***
contrast	4.95 ± 0.22	4.42 ± 0.50	4.42 ± 0.57	0.000	1.000
sharpness	4.85 ± 0.37	4.39 ± 0.62	4.21 ± 0.68	1.291	0.197
pulmonary vascular	4.86 ± 0.32	4.27 ± 0.87	4.61 ± 0.63	2.626	0.047
pulmonary airways	4.93 ± 0.26	4.14 ± 0.82	4.76 ± 0.48	3.142	0.032
artifacts	4.55 ± 0.60	4.03 ± 0.42	3.71 ± 0.65	2.324	0.020
overall image quality	4.60 ± 1.18	4.42 ± 0.57	4.17 ± 0.72	1.941	0.052

VIBE, volumetric interpolated breath-hold examination; UTE, ultrashort echo time; *, p-values were calculated using the Wilcoxon test between radial VIBE sequences and spiral UTE

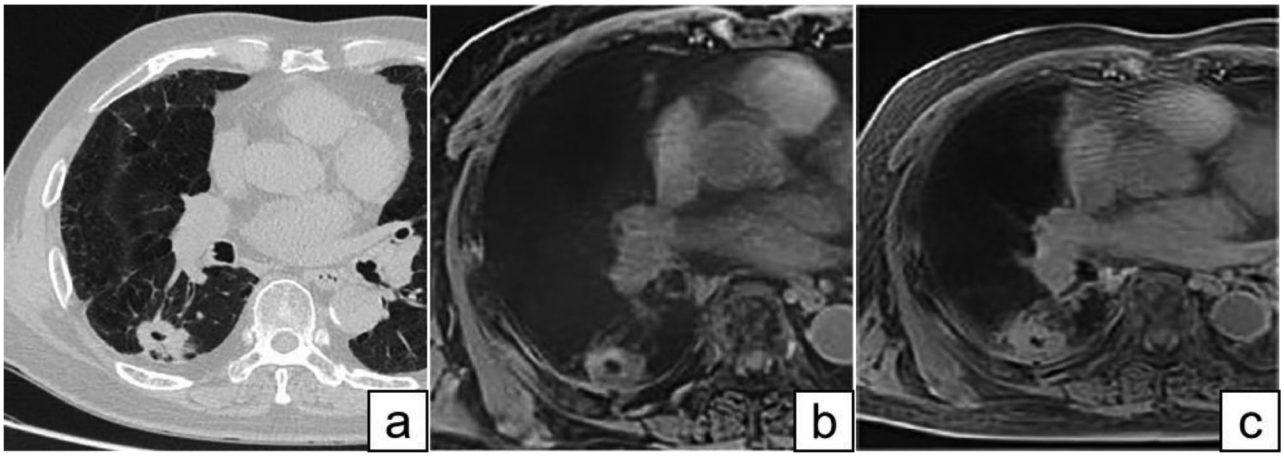

Fig. 1 Image quality assessment of CT and MRI sequences. A man presented with a lung nodule. CT (**a**), radial VIBE (**b**), and spiral UTE (**c**) clearly demonstrated the pulmonary nodule located in the lower lobe of the right lung; however, the pulmonary blood vessels were not well visualized

Table 5 Characteristics and detection rate of pulmonary nodules

Detection rate	Radial VIBE	Spiral UTE	χ^2
Number of nodules per size category			
diameter≤6 mm	39.13% (9/23)	82.61% (19/23)	5.818*
6 < diameter < 10 mm	63.64% (14/22)	90.91% (20/22)	3.125
diameter ≥ 10 mm	83.78% (31/37)	89.19% (33/37)	0.125
Number of nodules per location			
RUL	52.38% (11/21)	80.95% (17/21)	3.125
RML	53.85% (7/13)	69.23% (9/13)	0.100
RLL	78.95% (15/19)	94.74% (18/19)	0.800
LUL	66.67% (14/21)	95.24% (20/21)	2.286
LLL	87.50% (7/8)	100% (8/8)	0.000
Number of nodules per morphology category			
Solid	93.18% (41/44)	94.45% (42/44)	0.000
Part-solid	80.00% (8/10)	90.00% (9/10)	0.000
Non-solid	17.86% (5/28)	75.00% (21/28)	12.500*

RUL, right upper lung; RML, right middle lung; RLL, right lower lung; LUL, left upper lung; LLL, left lower lung; * McNemar tests evaluated differences between radial VIBE sequences and spiral UTE images, $p < 0.05$ indicated statistical significance

and CT was 0.99 ($P < 0.001$), while the Pearson correlation coefficient (r) between spiral UTE and CT was also 0.99 ($P < 0.001$). Figure 3 illustrates the evaluation of nodule size measurement between CT and MR images using linear regression analysis.

Agreement analysis of nodule size measurements

The inter-reader reliability for nodule diameter measurements using radial VIBE (ICC = 0.995) and spiral UTE (ICC = 0.996) sequences demonstrated good agreement ($P < 0.05$). The Bland–Altman plots illustrating inter-reader agreement are presented in Fig. 4A and B. Nodule size measurements were consistent between CT and MR images. Specifically, nodule size measurements for radial VIBE and spiral UTE images, when compared to CT images, were underestimated by 0.62 ± 0.99 mm (95% limits of agreement: −1.13 to 2.36 mm) and 0.34 ± 0.71 mm (95% limits of agreement: −1.05 to 1.72 mm), respectively. The Bland–Altman plots illustrating inter-modality agreement are shown in Fig. 4C and D.

Discussion

In this study, we found that the detection rates of ground glass nodules and nodules smaller than 6 mm were higher in the spiral UTE sequence compared to the radial VIBE sequence. Regarding image quality, the spiral UTE sequence outperformed the radial VIBE sequence in visualizing pulmonary vasculature and airways; however, the artifacts present in the radial VIBE images were significantly less pronounced than those in the spiral UTE sequence. Furthermore, the nodule sizes measured using the spiral UTE and radial VIBE sequences demonstrated a high degree of consistency with CT measurement.

One of the distinct advantages of the radial acquisition scheme is its significantly lower sensitivity to motion. Additionally, the overlap of radial spokes at the center of k-space yields a time-averaging effect that further diminishes sensitivity to motion and flow [16]. Consequently, the radial VIBE sequence exhibits fewer artifacts compared to the UTE sequence, which employs two K-space acquisition methods: radial and spiral acquisition. Some studies have indicated that radial UTE results in fewer artifacts than spiral UTE; however, the evaluation of nodules is superior with spiral UTE [17]. Furthermore, certain studies have demonstrated that spiral UTE images can effectively display sub-segmental pulmonary bronchi [14]. Darcot et al. [17]found that spiral UTE images clearly depict the peripheral vascular system. Our research also indicates that the radial VIBE sequence exhibits fewer image motion artifacts due to the radial acquisition. Conversely, while UTE sequence images obtained through spiral acquisition tend to have more artifacts, they provide clearer visualization of bronchi and blood vessels compared to radial VIBE.

We compared the detection rates of two sequences and found that the detection rates for radial VIBE and spiral UTE were 65.85% and 87.80%, respectively. Yu et al. [13] reported a nodule detection rate of 95.7% for the radial VIBE sequence; however, their study focused exclusively on one ground glass nodule. In contrast, Feng et al. [18] found a detection rate of 54.8% for the radial VIBE sequence, with a detection rate of 16.4% specifically for ground glass nodules. UTE has emerged as a promising technique, demonstrating a high-resolution lung MRI with pulmonary nodule detection rates ranging from 73.2–93.0% [19–21]. Renz et al. [15] and Olthof et al. [22] reported detection rates of 74% and 67%, respectively, for spiral UTE in nodules smaller than 7 mm. Similarly, Cha et al. [14]reported a detection rate of 88% for spiral UTE in nodules below 7 mm, aligning with our findings. The variability in detection rates may be attributed to differences in examination protocols,

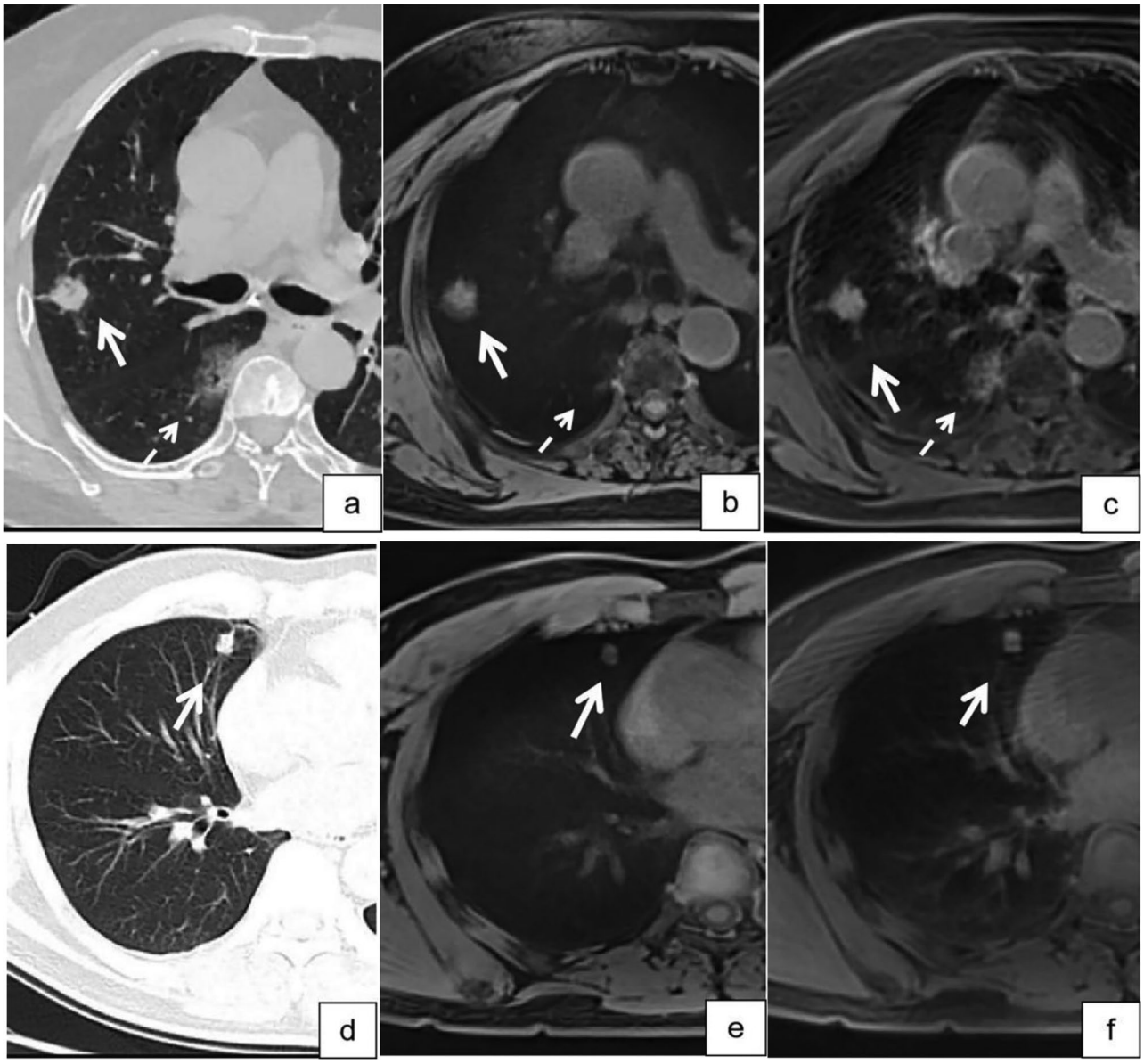

Fig. 2 The ability of different MRI sequences to detect nodules. A solid nodule measuring 12.1 mm (indicated by the white solid arrow) was identified in the right lung on CT (**a**), radial VIBE (**b**), and spiral UTE (**c**). Additionally, a ground glass nodule measuring 25.4 mm (indicated by the white dotted arrow) was also detected in the right lung on CT (**a**). When compared to radial VIBE (**b**), the ground glass nodule is more clearly visualized in the spiral UTE (**c**). Furthermore, another solid nodule measuring 10.5 mm (indicated by the white solid arrow) was observed on CT (**d**) and can also be detected using radial VIBE (**e**) and spiral UTE (**f**)

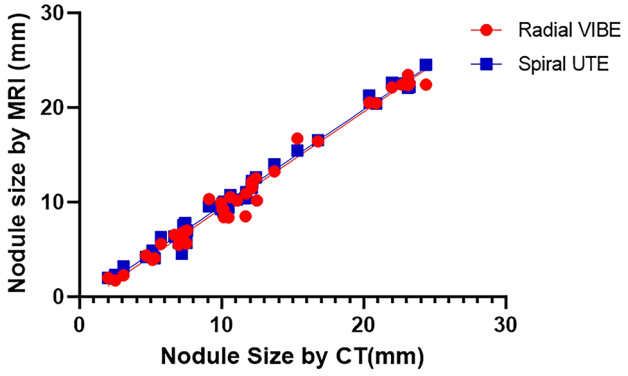

Fig. 3 Accuracy of nodule size in different MRI sequences. This study examines the associations between nodule size measurements obtained from CT and MRI images. Scatterplots illustrating these associations include data from radial VIBE and spiral UTE sequences. Radial VIBE and spiral UTE have good correlation with CT

such as slice thickness and MRI field strength. Our study showed the detection rate for ground glass nodules using the spiral UTE sequence was 75%, consistent with the findings of Ohno et al. [23]and Huang et al. [24]. However, the spiral UTE sequence employs end-expiratory diaphragm navigation technology for imaging, while CT image acquisition occurs at the end of the inspiratory breath, which can lead to a reduction in the volume of ground glass nodules and an increase in their density [23]. Additionally, we found that nodules located in regions adjacent to the heart, diaphragm, and peri-hilum are more likely to be clearly visualized on spiral UTE images.

Nodule size is critical for the management, diagnosis, and treatment of pulmonary nodules, as well as for TNM staging of lung cancer. In our study, the radial VIBE and spiral UTE sequence underestimated nodule size. A minor inter-reader bias was noted in MRI images regarding nodule size measurements, consistent with prior reports [14, 22, 23]. Additionally, the nodule size measured by CT is slightly larger than that measured by MRI. This study does have certain limitations. Firstly, we did not calculate the rates of true positives, false positives, false negatives, and true negatives. Secondly, the difference in thickness impacts the comparability of detection rates between the two sequences. However, utilizing a thinner layer thickness may prolong image acquisition time and cause discomfort for patients. Lastly, while we evaluated the detection and classification capabilities of the two methods, we did not assess nodule characteristics such as shape, border, location, or pleural indentation.

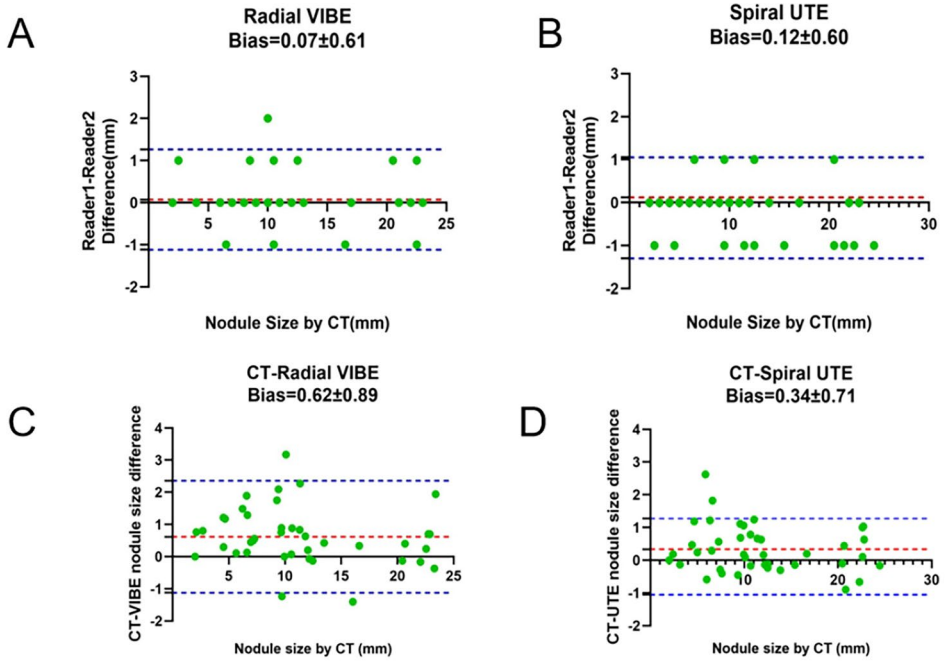

Fig. 4 Inter-reader and inter-methods agreement of CT and MR imaging. Bland–Altman plots illustrate the inter-reader agreement for nodule measurements obtained via CT and MR imaging. Minor inter-reader biases were noted for radial VIBE imaging (**A**) and spiral UTE imaging (**B**). In comparison to reference CT measurements, both radial VIBE imaging (**C**) and spiral UTE imaging (**D**) exhibited a bias towards underestimating nodule size

Conclusions

In summary, the spiral UTE sequence demonstrates superior efficacy compared to the radial VIBE sequence in the detection of ground glass nodules, as well as in the visualization of blood vessels and airways. This indicates that the spiral UTE sequence is particularly advantageous for patients with ground glass nodules. Additionally, radial VIBE sequences are characterized by their shorter acquisition times and reduced artifacts. The nodule sizes measured using both the spiral UTE and radial VIBE sequences are consistent with those obtained from CT imaging. This consistency suggests that MRI sequences may be effectively utilized for long-term radiotherapy and the management of patients with nodules, as well as for lung cancer staging.

Abbreviations

MRI	Magnetic resonance imaging
UTE	Ultrashort echo time
Spiral UTE	Spiral ultrashort echo time
Radial VIBE	Radial volumetric interpolated breath-hold examination
T2WI	T2-weighted imaging
T1WI	T1-weighted imaging
GRE	Three-dimensional gradient echo
HASTE	Half-fourier acquisition single-shot turbo spin-echo

Acknowledgements

Not applicable.

Author contributions

Yehai Jiang, Doudou Pu and Xuyang Zhang interpreted the patient data regarding the clinical information and the imaging analysis. Zhanli Ren and Nan Yu performed the CT and MRI analysis. Yehai Jiang and Nan Yu were a major contributor in writing the manuscript. All authors read and approved the final manuscript.

Funding

This study was supported by the Basic Research Program of Natural Science of Shaanxi Province (No: 2022 JM-453) and the National Innovation and Entrepreneurship Training Program for College Students (No:202210716013). The funding bodies played no role in the design of the study and collection, analysis, and interpretation of data and in writing the manuscript.

Data availability

Data is provided within the manuscript.

Declarations

Ethics approval and consent to participate

All procedures conducted in studies involving human participants adhered to the ethical standards set forth by the institutional and/or national research committee, as well as the Helsinki Declaration and its subsequent amendments or comparable ethical standards. This study received approval from the institutional review board of the affiliated hospital of Shaanxi University of Chinese Medicine, and all participating patients provided informed consent.

Consent for publication

Not applicable.

Competing interests

The authors declare no competing interests.

Author details

[1]School of Medical Technology, Shaanxi University of Chinese Medicine, Xian Yang 712046, China
[2]Department of Medical Imaging, Affiliated Hospital of Shaanxi University of Chinese Medicine, Xian Yang 712000, China
[3]Radiotherapy Department, The Second Affiliated Hospital of South China University, Heng Yang 421099, China

Received: 19 July 2023 / Accepted: 16 December 2024
Published online: 10 January 2025

References

1. Bortolotto C, Messana G, Lo Tito A, et al. The role of native T1 and T2 mapping Times in identifying PD-L1 expression and the histological subtype of NSCLCs[J]. Cancers (Basel). 2023;15(12). https://doi.org/10.3390/cancers15123252.
2. Ohno Y, Ozawa Y, Koyama H, et al. State of the art MR Imaging for Lung Cancer TNM Stage Evaluation[J]. Cancers (Basel). 2023;15(3). https://doi.org/10.3390/cancers15030950.
3. Sanchez F, Tyrrell PN, Cheung P, et al. Detection of solid and subsolid pulmonary nodules with lung MRI: performance of UTE, T1 gradient-echo, and single-shot T2 fast spin echo[J]. Cancer Imaging. 2023;23(1):17. https://doi.org/10.1186/s40644-023-00531-4.
4. Darçot E, Jreige M, Rotzinger DC, et al. Comparison between Magnetic Resonance Imaging and computed tomography in the detection and Volumetric Assessment of Lung nodules: a prospective Study[J]. Front Med (Lausanne). 2022;9:858731. https://doi.org/10.3389/fmed.2022.858731.
5. Alabed S, Garg P, Alandejani F, et al. Establishing minimally important differences for cardiac MRI endpoints in pulmonary arterial hypertension[J]. Eur Respir J. 2023. https://doi.org/10.1183/13993003.02225-2022.
6. Heidenreich JF, Kuhl PJ, Grunz JP, et al. Lung function in patients with cystic fibrosis before and during CFTR-Modulator therapy using 3D Ultrashort Echo Time MRI[J]. Radiology. 2023;308(1):e230084. https://doi.org/10.1148/radiol.230084.
7. Wei S, Lu R, Zhang Z, et al. MRI-assessed diaphragmatic function can predict frequent acute exacerbation of COPD: a prospective observational study based on telehealth-based monitoring system[J]. BMC Pulm Med. 2022;22(1):438. https://doi.org/10.1186/s12890-022-02254-x.
8. Tibiletti M, Eaden JA, Naish JH, et al. Imaging biomarkers of lung ventilation in interstitial lung disease from (129)xe and oxygen enhanced (1)H MRI[J]. Magn Reson Imaging. 2023;95:39–49. https://doi.org/10.1016/j.mri.2022.10.005.
9. Kumar S, Rai R, Moses D, et al. MRI in radiotherapy for lung cancer: a free-breathing protocol at 3T[J]. Pract Radiat Oncol. 2017;7(3):e175–83. https://doi.org/10.1016/j.prro.2016.10.008.
10. Kim TJ, Kim CH, Lee HY, et al. Management of incidental pulmonary nodules: current strategies and future perspectives[J]. Expert Rev Respir Med. 2020;14(2):173–94. https://doi.org/10.1080/17476348.2020.1697853.
11. Bruckmann NM, Kirchner J, Morawitz J, et al. Free-breathing 3D stack of stars GRE (StarVIBE) sequence for detecting pulmonary nodules in (18)F-FDG PET/MRI[J]. EJNMMI Phys. 2022;9(1):11. https://doi.org/10.1186/s40658-022-00439-1.
12. Huang YS, Niisato E, Su MM, et al. Detecting small pulmonary nodules with spiral ultrashort echo time sequences in 1.5 T MRI[J]. Magma. 2021;34(3):399–409. https://doi.org/10.1007/s10334-020-00885-x.
13. Yu N, Duan H, Yang C, et al. Free-breathing radial 3D fat-suppressed T1-weighted gradient echo (r-VIBE) sequence for assessment of pulmonary lesions: a prospective comparison of CT and MRI[J]. Cancer Imaging. 2021;21(1):68. https://doi.org/10.1186/s40644-021-00441-3.
14. Cha MJ, Ahn HS, Choi H, et al. Accelerated stack-of-spirals free-breathing three-Dimensional Ultrashort Echo Time Lung magnetic resonance imaging: a feasibility study in patients with breast Cancer[J]. Front Oncol. 2021;11:746059. https://doi.org/10.3389/fonc.2021.746059.
15. Renz DM, Herrmann KH, Kraemer M, et al. Ultrashort echo time MRI of the lung in children and adolescents: comparison with non-enhanced computed tomography and standard post-contrast T1w MRI sequences[J]. Eur Radiol. 2022;32(3):1833–42. https://doi.org/10.1007/s00330-021-08236-7.
16. Chandarana H, Block TK, Rosenkrantz AB, et al. Free-breathing radial 3D fat-suppressed T1-weighted gradient echo sequence: a viable alternative for contrast-enhanced liver imaging in patients unable to suspend respiration[J]. Invest Radiol. 2011;46(10):648–53. https://doi.org/10.1097/RLI.0b013e31821eea45.

17. Darçot E, Delacoste J, Dunet V, et al. Lung MRI assessment with high-frequency noninvasive ventilation at 3 T[J]. Magn Reson Imaging. 2020;74:64–DOI73. https://doi.org/10.1016/j.mri.2020.09.006.
18. Feng H, Shi G, Liu H, et al. The application and value of 3T magnetic resonance imaging in the Display of Pulmonary Nodules[J]. Front Oncol. 2022;12:844514. https://doi.org/10.3389/fonc.2022.844514.
19. Cha M, Park H, Paek M, et al. Free-breathing ultrashort echo time lung magnetic resonance imaging using stack-of-spirals acquisition: a feasibility study in oncology patients[J]. Magn Reson Imaging. 2018;51:137–43. https://doi.org/10.1016/j.mri.2018.05.002.
20. Ohno Y, Koyama H, Yoshikawa T, et al. Standard-, Reduced-, and No-Dose Thin-Section Radiologic examinations: comparison of capability for Nodule Detection and Nodule Type Assessment in patients suspected of having pulmonary Nodules[J]. Radiology. 2017;284(2):562–73. https://doi.org/10.1148/radiol.2017161037.
21. Bae K, Jeon KN, Hwang MJ, et al. Comparison of lung imaging using three-dimensional ultrashort echo time and zero echo time sequences: preliminary study[J]. Eur Radiol. 2019;29(5):2253–62. https://doi.org/10.1007/s00330-018-5889-x.
22. Olthof SC, Reinert C, Nikolaou K, et al. Detection of lung lesions in breath-hold VIBE and free-breathing spiral VIBE MRI compared to CT[J]. Insights Imaging. 2021;12(1):175. https://doi.org/10.1186/s13244-021-01124-0.
23. Ohno Y, Takenaka D, Yoshikawa T, et al. Efficacy of Ultrashort Echo Time Pulmonary MRI for Lung Nodule Detection and Lung-RADS Classification[J]. Radiology. 2022;302(3):697–706. https://doi.org/10.1148/radiol.211254.
24. Huang YS, Niisato E, Su MM, et al. Applying compressed sensing volumetric interpolated breath-hold examination and spiral Ultrashort Echo Time sequences for lung nodule detection in MRI[J]. Diagnostics (Basel). 2021;12(1). https://doi.org/10.3390/diagnostics12010093.

Publisher's note